

Article

A Non-Tuned Machine Learning Technique for Abutment Scour Depth in Clear Water Condition

Hossein Bonakdari ^{1,*}, Fatemeh Moradi ², Isa Ebtehaj ², Bahram Gharabaghi ³,
Ahmed A. Sattar ^{4,5}, Amir Hossein Azimi ⁶ and Artur Radecki-Pawlik ⁷

¹ Department of Soils and Agri-Food Engineering, Laval University, Québec, QC G1V 0A6, Canada

² Environmental Research Center, Razi University, Kermanshah 6714414971, Iran;
f.moradi23@yahoo.com (F.M.); isa.ebtehaj@gmail.com (I.E.)

³ School of Engineering, University of Guelph, Guelph, ON N1G 2W1, Canada; bgharaba@uoguelph.ca

⁴ Department of Irrigation & Hydraulics, Faculty of Engineering, Cairo University, Giza 12316, Egypt;
ahmoudy77@yahoo.com

⁵ Faculty of Civil Engineering, German University in Cairo, New Cairo 13611, Egypt

⁶ Department of Civil Engineering, Lakehead University, Thunder Bay, ON P7B 5E1, Canada;
azimi@lakeheadu.ca

⁷ Division of Structural Mechanics and Material Mechanics, Faculty of Civil Engineering,
Cracow University of Technology, 31-155 Krakow, Poland; rmradeck@cyf-kr.edu.pl

* Correspondence: hossein.bonakdari@fsaa.ulaval.ca; Tel.: +1-418-656-2131; Fax: +1-418-656-3723

Received: 8 December 2019; Accepted: 16 January 2020; Published: 20 January 2020



Abstract: Abutment scour is a complex three-dimensional phenomenon, which is one of the leading causes of marine structure damage. Structural integrity is potentially attainable through the precise estimation of local scour depth. Due to the high complexity of scouring hydrodynamics, existing regression-based relations cannot make accurate predictions. Therefore, this study presented a novel expansion of extreme learning machines (ELM) to predict abutment scour depth (d_s) in clear water conditions. The model was built using the relative flow depth (h/L), excess abutment Froude number (F_e), abutment shape factor (K_s), and relative sediment size (d_{50}/L). A wide range of experimental samples was collected from the literature, and data was utilized to develop the ELM model. The ELM model reliability was evaluated based on the estimation results and several statistical indices. According to the results, the sigmoid activation function (correlation coefficient, $R = 0.97$; root mean square error, $RMSE = 0.162$; mean absolute percentage error, $MAPE = 7.69$; and scatter index, $SI = 0.088$) performed the best compared with the hard limit, triangular bias, radial basis, and sine activation functions. Eleven input combinations were considered to investigate the impact of each dimensionless variable on the abutment scour depth. It was found that $d_s/L = f(F_e, h/L, d_{50}/L, K_s)$ was the best ELM model, indicating that the dimensional analysis of the original data properly reflected the underlying physics of the problem. Also, the absence of one variable from this input combination resulted in a significant accuracy reduction. The results also demonstrated that the proposed ELM model significantly outperformed the regression-based equations derived from the literature. The ELM model presented a fundamental equation for abutment scours depth prediction. Based on the simulation results, it appeared the ELM model could be used effectively in practical engineering applications of predicting abutment scour depth. The estimated uncertainty of the developed ELM model was calculated and compared with the conventional and artificial intelligence-based models. The lowest uncertainty with a value of ± 0.026 was found in the proposed model in comparison with ± 0.50 as the best uncertainty of the other models.

Keywords: abutment; clear water; equation; sensitivity analysis; scour

1. Introduction

The presence of hydraulic structures obstructs the flow and leads to subsequent scour around structure foundations. Scour is recently recognized as the most common cause of bridge foundation failure, leading to property losses, business failure, and the disruption of economic activities [1,2]. For accurate scour depth prediction, knowledge of scouring is necessary. Scour depth overestimation and underestimation lead to higher construction costs and abutment foundation damage, respectively [3–5]. Hence, an accurate method of predicting scour depth is necessary to reduce economic costs and achieve high-stability confidence coefficients for foundations.

When river flow comes in contact with bridge abutments, the pressure creates a downward flow around the structures. This downward flow forms bed cavities containing vortices. Shear stress-generated upstream of an abutment leads to primary vortices, which withdraw to the abutment and create secondary vortices that are less able than the initial vortices. Besides, unstable shear layers produced according to the separation of flow upstream and downstream of bridge abutments rotate in the form of vortex structures known as wake vortices. Wake vortices act similarly to small eddies and sediment rising from the bed [6–9].

Numerous experimental studies have been done to survey the abutment scour and deposition process in clear water conditions [6,10–21]. Dey and Barbhuiya [22] proposed different regression-based equations based on the abutments' type as follows:

$$\frac{d_s}{L} = 7.281 (F_e^{0.314}) \left(\frac{h}{L}\right)^{0.128} \left(\frac{L}{d_{50}}\right)^{-0.167} \quad \text{Vertical – Wall} \quad (1)$$

$$\frac{d_s}{L} = 8.319 (F_e^{0.312}) \left(\frac{h}{L}\right)^{0.101} \left(\frac{L}{d_{50}}\right)^{-0.231} \quad \text{45° Wing – Wall} \quad (2)$$

$$\frac{d_s}{L} = 8.689 (F_e^{0.192}) \left(\frac{h}{L}\right)^{0.103} \left(\frac{L}{d_{50}}\right)^{-0.296} \quad \text{Semicircular} \quad (3)$$

Moreover, the conventional regression-based model of the Muzzammil [23] is defined as follows:

$$\frac{d_s}{L} = 9.694 K_s (F_e^{0.648}) \left(\frac{h}{L}\right)^{0.04} \left(\frac{d_{50}}{L}\right)^{-0.075} \quad (4)$$

where d_{50} denotes as the median diameter of sediment particles, d_s is the equilibrium scour depth, h is the approaching flow depth, L is the radius of scour hole at original bed level upstream, and F_e is the excess abutment Froude number, which is defined as:

$$F_e = \frac{U_e}{\sqrt{g(s-1)l}} \quad (5)$$

where l is the transverse length of an abutment, g is the acceleration due to gravity, U_e is the excess approaching flow velocity, and s is the relative density of sediment particles.

The majority of studies offer several empirical equations that are highly dependent on experimental conditions; hence, the results obtained with various methods differ significantly. There is much disagreement on the selection of a comprehensive approach to designing bridge abutments that are protected against scour. Moreover, the equations obtained cannot serve as general and reliable equations for estimating bridge abutment scour [24,25].

Various studies have addressed scour prediction using feedforward neural networks (FFNN) [26]; gene expression programming (GEP) [27–29]; adaptive neuro-fuzzy inference systems (ANFIS) [30]; support vector machines (SVM) [31]; group method of data handling (GMDH) [32–35], and model trees [36].

Bateni and Jeng [37] applied an ANFIS-based method to estimate the scour at pile groups. They found that the ANFIS model outperformed conventional techniques. Muzzammil [38] employed a neural network to evaluate the scour at abutments and concluded that neural networks could serve as alternative experimental and regression methods for predicting the complex flow structures around bridge abutments. Their artificial neural network (ANN) model produced better results than a conventional regression model. The raw parameters also exhibited superior performance to dimensionless parameters in scour prediction. Ghani and Azamathulla [39] employed an ANFIS model to investigate the scour process at culvert outlets. They found that ANFIS predicted scour depth more accurately than artificial neural networks and regression equations.

Begum [40] employed an ANN model to estimate the scour depth around semi-circular bridge abutments. They applied sensitivity analysis to the input parameters to investigate the impact of each independent variable and determined that the ANN model was more precise than other experimental formulas available. Azamathulla [28] used gene-expression programming (GEP) and artificial neural network (ANN) models to assess the scour process at bridge abutments. According to the findings, the GEP model produced more satisfactory results compared to the ANN model in predicting scour depth. Etemad-Shahidi et al. [36] employed model trees (MT) and evaluated datasets with a broad range of variables for predicting scour around circular piers. In terms of relative scour depth prediction, their model was presented as a function of Froude number, relative flow depth, and flow velocity. The model tree (MT) results were compared with an experimental formula, and it was found that the MT could estimate scouring depth more accurately.

One of the most popular techniques for scour depth prediction is the feedforward neural networks (FFNN). It has recently been employed as a classic method in data mining to validate the superiority of artificial intelligence methods, such as ANFIS, extreme learning machine (ELM), ANN, etc. [26,41–45]. The classic FFNN is trained with a backpropagation algorithm. The ANFIS, which is a combination of neural network and fuzzy logic, is employed by Moradi et al. [46] to calculate the abutment scour depth. The authors compared different techniques for generating the fuzzy inference systems (FIS) (i.e., sub-clustering (SC), fuzzy c-means clustering (FCM), and grid partitioning (GP)). The results indicated that the ANFIS-SC outperformed all other existing ANFIS techniques. Besides, Azimi et al. [47] proposed a multi-objective design of ANFIS optimized by genetic algorithm. The authors indicated that this technique not only provided more accurate results but also enhanced the generalizability of the ANFIS model in abutment scour depth prediction. The main problems of the mentioned ANFIS-based techniques are the failure to provide a specific relationship to apply in practical tasks.

The shortcomings of feedforward neural networks back propagation (FFNN-BP) are the low learning rate, the slow convergence rate, and the presence of local minima [48]. Besides, other artificial intelligence-based methods like ANFIS are black-box methods, which do not yield equations for use in practical work. Classification-based methods, such as model trees (MT), classify data, and, in particular, conditions yield equations. However, the main problems with such methods are the lack of flexibility and adequate performance in different hydraulic conditions. Although the GEP method provides an equation for use in practical engineering problems, the problems with this method are the high central processing unit (CPU) time consumption and that the equations presented are often achieved using several highly sophisticated functions.

For these reasons, Huang et al. [49] proposed a new algorithm, the extreme learning machine (ELM), for FFNN training based on single hidden layer feedforward neural networks (SLFNs). ELM requires adjusting only the activation function type and some hidden layers, while there are several user-defined parameters, such as hidden layer bias adjustment, during algorithm and input weight adjustment [50]. Moreover, using ELM leads to produce equations for practical problems [51].

Compared to other learning algorithms, such as back propagation (BP), ELM achieves swift learning and performs well in generation function processing [52–55]. Using ELM in various engineering science fields, such as feature selection [56], classification [57], and regression [51,58], has provided acceptable results.

Since ELM has not been used for scour depth modeling, this method was applied here to predict the abutment scour depth in clear water conditions. This approach overcame many issues in modeling scour depth by using the existing artificial intelligence methods. For this purpose, the parameters affecting the abutment scour depth were determined first. Then, different activation functions were considered in predicting the abutment scour depth. Upon selecting the best activation function and carrying out a dimensional analysis, the influence of each parameter affecting the scour depth was evaluated from eleven input combinations. Moreover, the current study results and two empirical formulae were compared with previous studies. Finally, the optimum combination was used to present a relationship for practical engineering problems.

2. Materials and Methods

2.1. Data Collection

To estimate the scour depth around bridge abutments in clear water with a uniform sediment bed, a set of 295 experimental data were collected from the study of Dey and Barbhuiya [22]. They performed experiments in a lab flume ($20 \times 0.7 \times 0.9$ m long, deep, and wide) using a vertical wall, 45° wing-wall, and semicircular abutments, which are schematically illustrated in Figure 1.

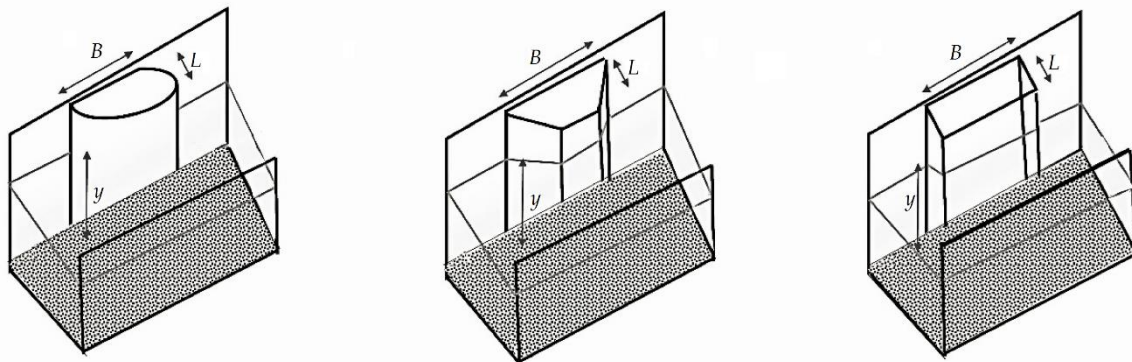


Figure 1. Schematic of the different abutment in the flume. L and B are the abutment length and width respectively.

During the tests, an abutment was set in the bed, sustained by a sediment intromission 0.3 m deep, 2.4 m long, and 0.9 m wide, and appended to the flume sidewall. Recess sediments were placed 9 m downstream of the flume, and the discharge was adjusted by the entrance inlet. The flow depth was measured using a Vernier point gauge with ± 0.1 mm accuracy. All tests were done in clear water conditions and $U/U_c = 0.95$, where U_c is the critical velocity of bed particles. Table 1 presents the sediment particle sizes, abutment geometric shapes, and flow conditions. Of the 295 experimental samples, approximately 50% of the samples were randomly selected for model training (148 samples), and the rest of the samples were applied for the testing stage (147 samples).

Table 1. Statistical indices for the collected dataset.

Variable	Min	Max	Mean	Variance	Standard Deviation
d_{50} (mm)	0.26	3.1	0.92	0.51	0.71
h (m)	0.05	0.25	0.16	0.004	0.06
U (m/s)	0.219	0.67	0.35	0.013	0.11
d_s (m)	0.024	0.293	0.13	0.003	0.06
L (m)	0.04	0.13	0.08	0.001	0.03
B (m)	0.08	0.36	0.18	0.006	0.08

Note: d_{50} is the average diameter of particles, h is the stream depth of approach, U is the average stream velocity, U_c is the critical velocity of sediment, d_s is the scour depth, L and B are the abutment length and width respectively.

2.2. Extreme Learning Machine

The ELM was first introduced by Huang et al. [49] as a new robust learning algorithm for single-layer feedforward neural networks (SLFNN). The ELM is very simple to use since only the network architecture should be defined. Hence, the ELM does not have the complexity of gradient algorithms, such as local minima, learning epochs, and learning rate. Moreover, it is proven that the speed of ELM is much greater than SVM and gradient-based algorithms, such as back-propagation. Thus, ELM training often takes a few seconds or a few minutes in very complex cases with important data where modeling with the classical neural network is not easy. In this algorithm, the weight vector is associated with the input and hidden layers. Moreover, the primary neurons in the hidden layer are generated randomly, and a unique optimal solution is produced to determine the number of hidden layer neurons during training. If m is the number of nodes in the input layer, M is the number of nodes in the hidden layer, n is the number of nodes in the output layer, b_i is the bias, and $g(x)$ is the activation function of neurons in the hidden layer, for N arbitrary separate samples (x_i, t_i) , $x_i = [x_{i1}, x_{i2}, \dots, x_{im}]^T \in R^m$, $t_i = [t_{i1}, t_{i2}, \dots, t_{in}]^T \in R^n$, model network training by ELM is presented as follows (Figure 2):

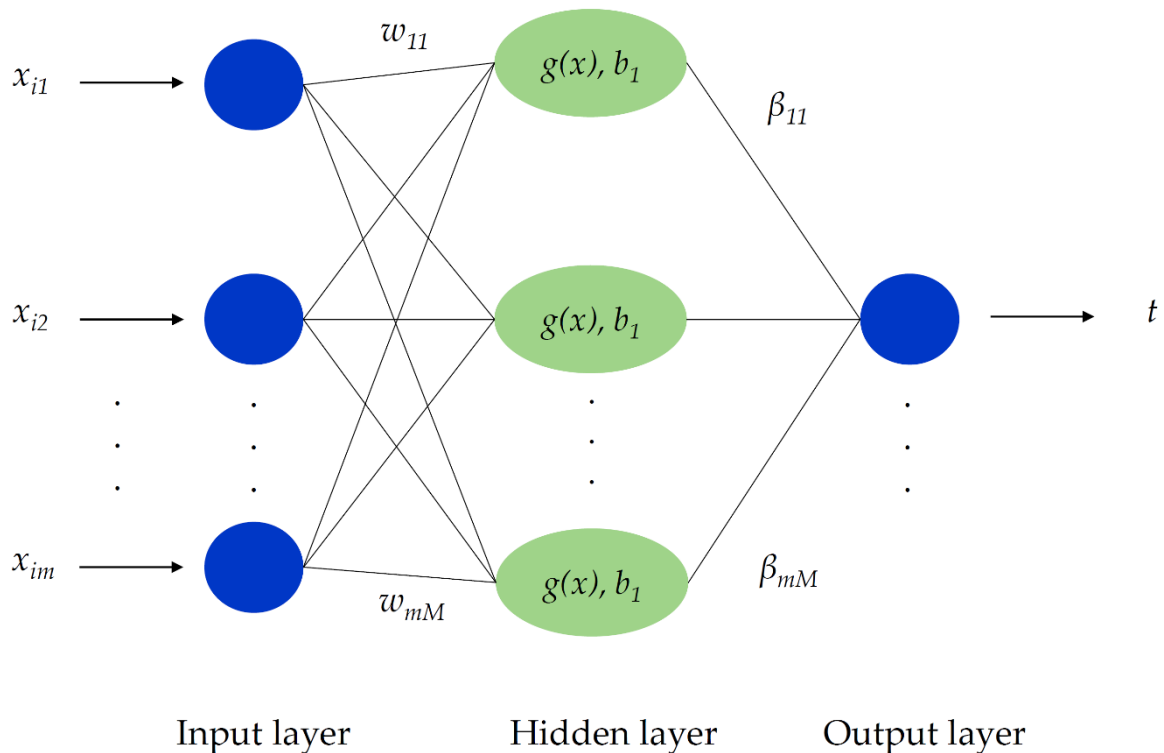


Figure 2. Extreme learning machine (ELM) structure.

The standard SLFNN forms with M neurons in the hidden layer, and activation function $g(x)$ is modeled as follows [59,60]:

$$\sum_{i=1}^M \beta_i g(W_i \cdot X_i + b_i) = O_j \quad j = 1, 2, \dots, N \quad (6)$$

where $O_i = [O_{i1}, O_{i2}, \dots, O_{in}]^T$ is the output vector from SLFNN, $W_i \cdot X_i$ is the inner product of X_i and W_i , b_i is the bias of the i th hidden layer neuron, $\beta_i = [\beta_{i1}, \beta_{i2}, \dots, \beta_{in}]^T$ is a gravimetric vector associated with the i th hidden layer neuron and output nodes, and $W_i = [W_{1i}, W_{2i}, \dots, W_{mi}]^T$ is the weight vector related to the hidden layer neuron and input nodes.

Activation functions are used to calculate the weight of neuron response output. The neurons consist of two parts, including the weighted sums of inputs and activation functions. When a set of weighted input signals is applied, activation functions are used to obtain the layer response. For neurons in the same layer, the same activity functions are used, which can be linear or nonlinear. In linear functions, a straight line is drawn, and in nonlinear functions, a curved line is drawn. The ELM nonlinear activity functions investigated in this study included hard limit sine, sigmoid, radial basis, and triangular basis: they are briefly defined as follows (see Figure 3):

- A sine function inserts the actual amount that has -1 to $+1$ efficiency.
- Sigmoid is a continuous function that gradually changes between asymptotic values of 0 and 1 or -1 and $+1$.
- When neurons use a hard limit transfer function, and if the input threshold net is gained, the output is 1 , otherwise 0 .
- The radial basis function output is based on the distance from the origin points.
- A triangular basis function can serve as a neuron transfer function. This function calculates the output layer from a given input layer.

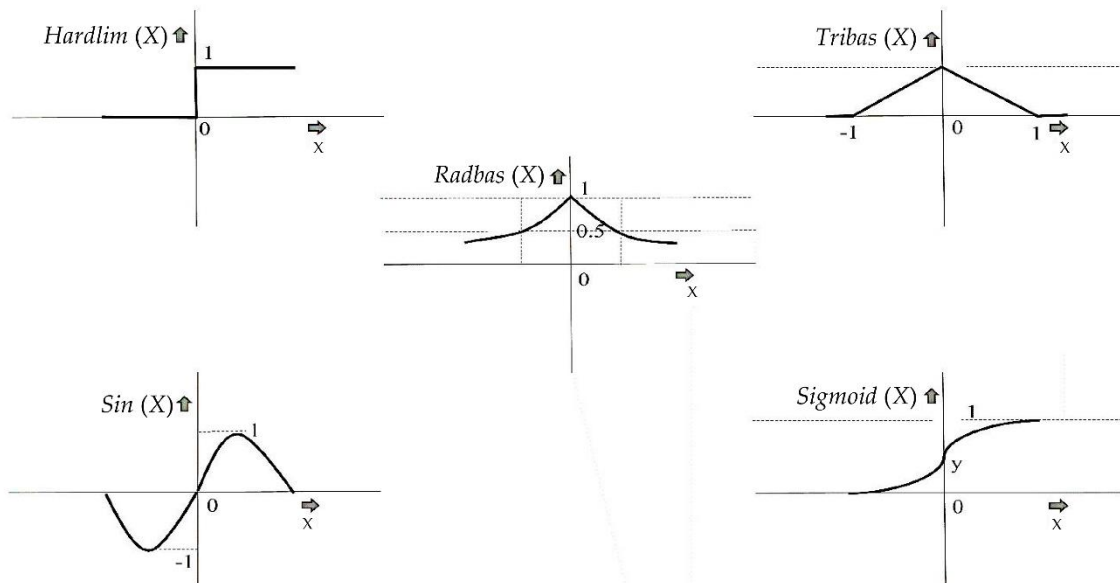


Figure 3. The different activation functions in the ELM model.

The standard SLFNN form with an activation function $g(x)$ and M hidden neurons can approximate all N samples with 0 error.

The relation between w_i , β_i , and b_i is defined as follows:

Equation (6) can be expressed in the form of the following matrix:

$$H\beta = Y \tag{7}$$

where H is the output matrix related to the hidden layer. When the input weights are selected randomly, and the hidden layer neurons are determined, the network training equivalent to the search for the least-squares ($\hat{\beta}$) related to Equation (7) is minimized as follows:

$$\min_{\beta} \|H\beta - Y\| \tag{8}$$

The smallest-norm least-squares solution is:

$$\hat{\beta} = \mathbf{H}^+ \mathbf{Y} \quad (9)$$

where \mathbf{H}^+ is the Moore–Penrose generalized inversion of hidden layer matrix \mathbf{H} .

Therefore, the ELM method is summarized in three steps:

- (i) Generate the hidden layer bias (b); randomly generate the weight vector (w) that links the input and hidden layers;
- (ii) Compute the hidden layer output matrix (H);
- (iii) Compute the output weight.

2.3. Methodology

Scour around abutments based on the flow's capacity to transfer bed materials is classified into two categories: moving bed scour and clear water scour. Moving bed scour when the flow moves the general bedload, while clear water scour happens when the flow does not move sediment downstream. The effective parameter on scour depth d_s at an abutment located on a bed with uniform sediment in clear water is a function of sediment characteristics, flow parameters, and hydraulic structure geometry [61–63].

$$d_s = f(U, U_c, L, g, K_s, d_{50}, h, \rho, \rho_s, \nu) \quad (10)$$

where U is the average stream velocity, U_c is the critical velocity of sediment, L is the abutment length, g is the gravitational acceleration, d_{50} is the average diameter of particles, h is the stream depth of approach, ρ and ρ_s represent the fluid and sediment density, respectively, and ν is the fluid kinematic velocity. The K_s is the abutment form factor that was determined by a trial-and-error procedure for the best collapsed of all data by Mellville [16]. It is 1 for vertical-wall abutments, 0.82 for 45° wing-wall abutments, and 0.75 for semicircular abutments. Dey and Barbhuiya [17] neglected the effect of viscosity and considered the relative density constant to express the following relationship:

$$d_s = f(U, U_c, L, g, K_s, d_{50}, h) \quad (11)$$

Abutment scour is occurred when the additional stream velocity U_e is greater than 0, where $U_e = U - \xi U_c$, and ξ is a constant coefficient for vertical wall, 45° wing-wall, and semicircular wall abutments of 0.5, 0.55, and 0.6, respectively.

$$d_s = f(U_e, L, g, K_s, d_{50}, h) \quad (12)$$

Most studies in the field of artificial intelligence consider the effective parameters in output parameter estimation to be dimensionless, which leads to good results [64–66]. According to the Buckingham Π theorem, the abutment scours depth is normalized as:

$$\frac{d_s}{L} = f\left(F_e, \frac{d_{50}}{L}, \frac{h}{L}, K_s, R_e\right) \quad (13)$$

where $F_e = U_e / \sqrt{\Delta g L}$ is the excess abutment Froude number and $\Delta = s - 1$, where s is the specific gravity of sediment, and R_e is Reynolds number. As the flow around an abutment is quite turbulent, the impact of R_e is neglected, and the following equation is ultimately recommended as:

$$\frac{d_s}{L} = f\left(F_e, \frac{d_{50}}{L}, \frac{h}{L}, K_s\right) \quad (14)$$

To predict the relative scour, the activation functions used in the ELM model were initially controlled to select the best one. Subsequently, the effect of each input variable on relative scours depth

in clear water condition (i.e., Equation (9)) was investigated. Various input parameter combinations were also evaluated, and the results are listed in Table 2.

Table 2. Different input combinations, containing the effective variables on abutment scour depth.

Model. No	Fe	h/L	d_{50}/L	K_s
ELM1				
ELM2				
ELM3				
ELM4				
ELM5				
ELM6				
ELM7				
ELM8				
ELM9				
ELM10				
ELM11				

Note: ELM, indicates extreme learning machine; relative flow depth (h/L); excess abutment Froude number (Fe); abutment shape factor (K_s); relative sediment size (d_{50}/L); green, blue and orange colors show the model with four, three and two inputs.

2.4. The Goodness of Fit Statistics

To evaluate the performance of each model presented in this study, scour depth was estimated using various statistical indices: correlation coefficient (R), root mean square error ($RMSE$), mean absolute percentage error ($MAPE$), and scatter index (SI), which are calculated as follows:

$$R = \frac{\sum_{i=1}^n (E_i - \bar{E})(M_i - \bar{M})}{\sqrt{\sum_{i=1}^n (E_i - \bar{E})^2 \sum_{i=1}^n (M_i - \bar{M})^2}} \tag{15}$$

$$RMSE = \sqrt{\left(\frac{1}{n}\right) \sum_{i=1}^n (E_i - M_i)^2} \tag{16}$$

$$MAPE = \left(\frac{100}{n}\right) \sum_{i=1}^n \left(\frac{|E_i - M_i|}{E_i}\right) \tag{17}$$

$$SI = \frac{RMSE}{\bar{E}} \tag{18}$$

where M_i and E_i are the modeled and experimented d_s/L values, respectively, and \bar{M} and \bar{E} are the mean modeled and experimented d_s/L values, respectively. Recently, a new goodness-of-fit index was defined by Eray et al. [67] as combined accuracy (CA). It is a combination of $RMSE$, MAE , and R^2 as follows:

$$CA = 0.33((1 - R^2) + MAE + RMSE) \tag{19}$$

where R^2 and MAE are determination coefficient and mean absolute error, respectively.

3. Results

The ELM activation functions' performance in predicting abutment scour depth in clear water was examined using Dey and Barbhuiya [22] dataset. According to Figure 4, it could be concluded that

the sigmoid activation function predicted scour around an abutment well ($R = 0.97$), whereby most data points had an average error below 8% ($MAPE = 7.69\%$) and the lowest data scattering ($SI = 0.088$).

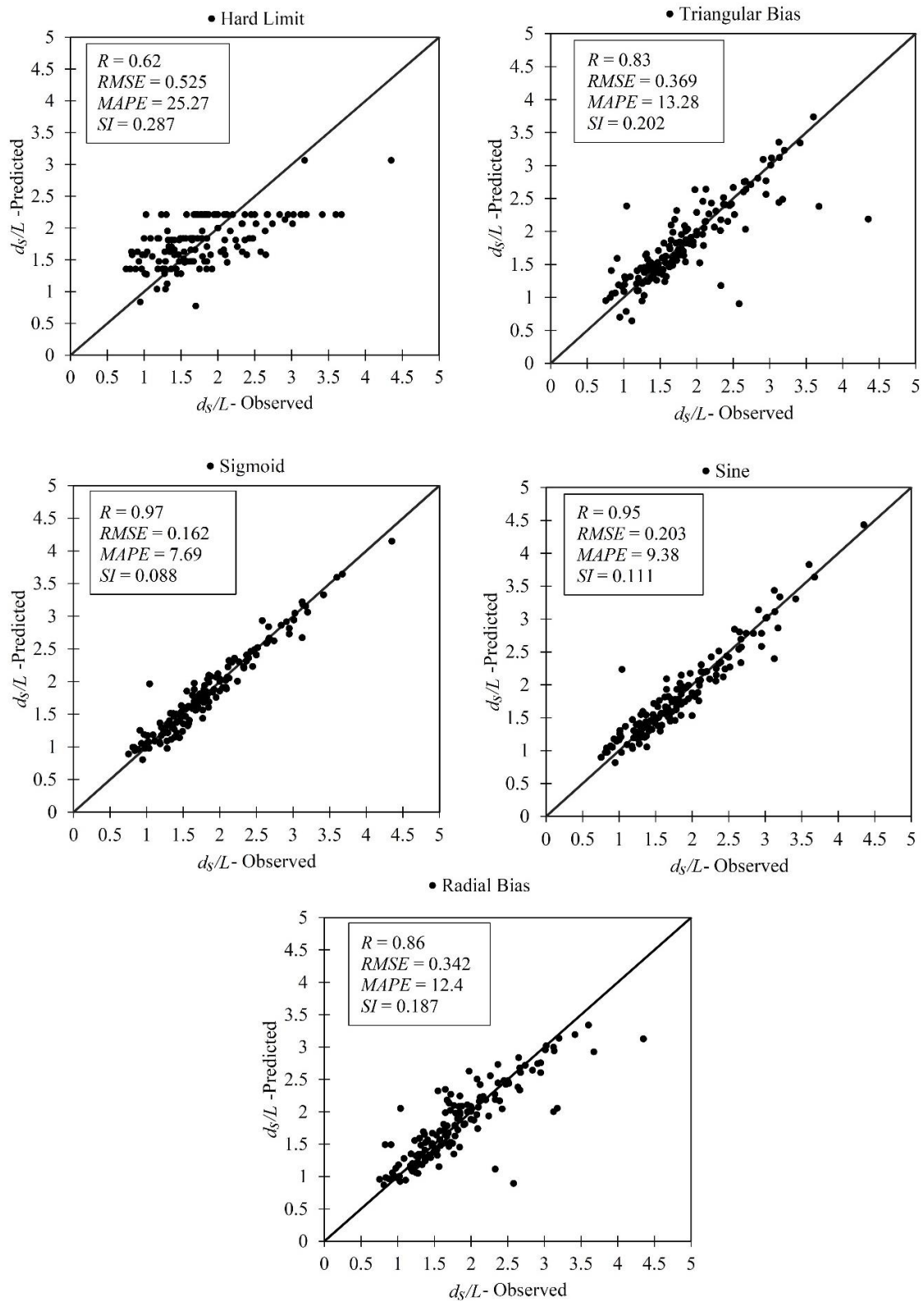


Figure 4. Scatter plot of different ELM activation functions.

The *MAPE* and *SI* of the sine activation function were over 2% and 4% higher than the sigmoid activation function, respectively, though the correlation coefficient for the sigmoid function had a small margin ($R = 0.95$). According to the statistical indices for the hard limit activation function, there was a significant difference between the estimated data points and the observed data ($R = 0.62$). Moreover, with an average error of 26% ($MAPE = 25.27$), the hard limit activation function had the highest error value among activation functions, signifying the poor performance of the hard limit activation function in scouring estimation. According to Figure 4, the mean error for the triangular basis and radial basis functions was 6% and 5% higher, respectively, than the sigmoid activation function. Therefore, the sigmoid activation function outperformed the other activation functions in scour depth estimation. The sigmoid function was, therefore, applied to abutment scour depth modeling with the input combinations presented in Table 2.

Figure 5 presents a comparison of 11 input combinations' performance (see Table 2) according to various statistical indices. The ELM1 input combination included all effective parameters on abutment scour depth in clear water conditions (Equation (14)). The ELM results exhibited greater ability in the prediction of the abutment scour depth by using the ELM1 input combination. This was because the difference between estimated and experimental data was negligible ($R = 0.97$), and the estimated values had less than 8% relative error ($MAPE = 7.69$). Besides, the relative error (RE) distributions in Figure 5 indicated that 46% and 74% of all samples were estimated with less than 5% and 10% (respectively) RE, and only 5% of samples were estimated with more than 20% RE, (see Tables S1 and S2 for more detail).

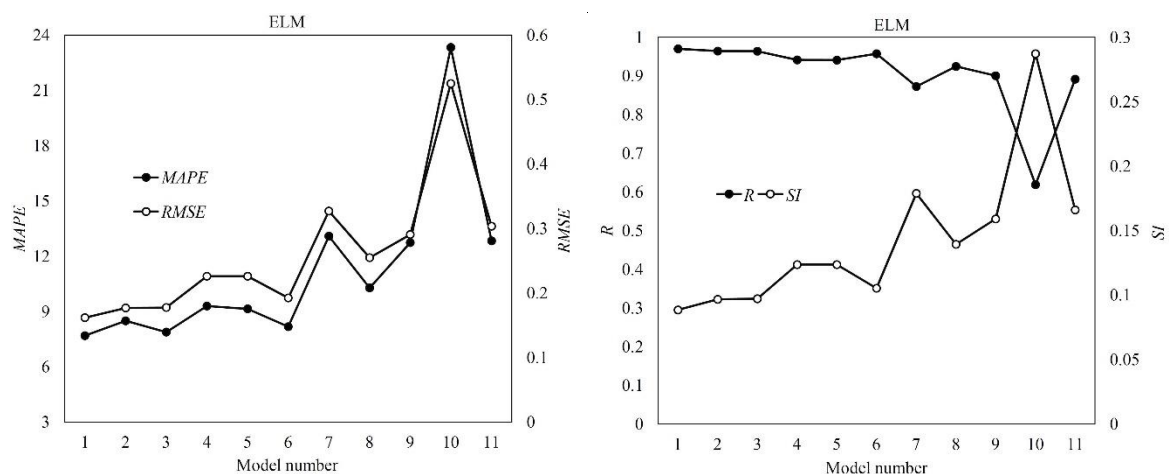


Figure 5. Comparison of different input combinations in abutment scours depth prediction.

Next, by neglecting various parameters at a time and assessing 10 new input combinations (ELM2 to ELM11), the effect of each parameter on d_s/L was examined, based on Equation (9). The input combinations ELM2 to ELM5 used three input parameters for predicting abutment scour depth. According to Figure 5, the R and SI values for ELM2 were 0.96 and 0.096, respectively. The difference between ELM2 and ELM1 was the absence of parameter K_s , which led to a higher mean relative error ($MAPE = 8.49$) compared to ELM1 ($MAPE = 7.69$). Besides, the RE distribution provided in Figure 5 demonstrated that ELM2 increased the RE distribution so that more than 74% estimated samples with less than 10% RE decreased to 67.46%. Consequently, the results indicated that neglecting the abutment geometry parameter in scour depth evaluation was significant, whereby ignoring it reduced d_s/L performance and accuracy.

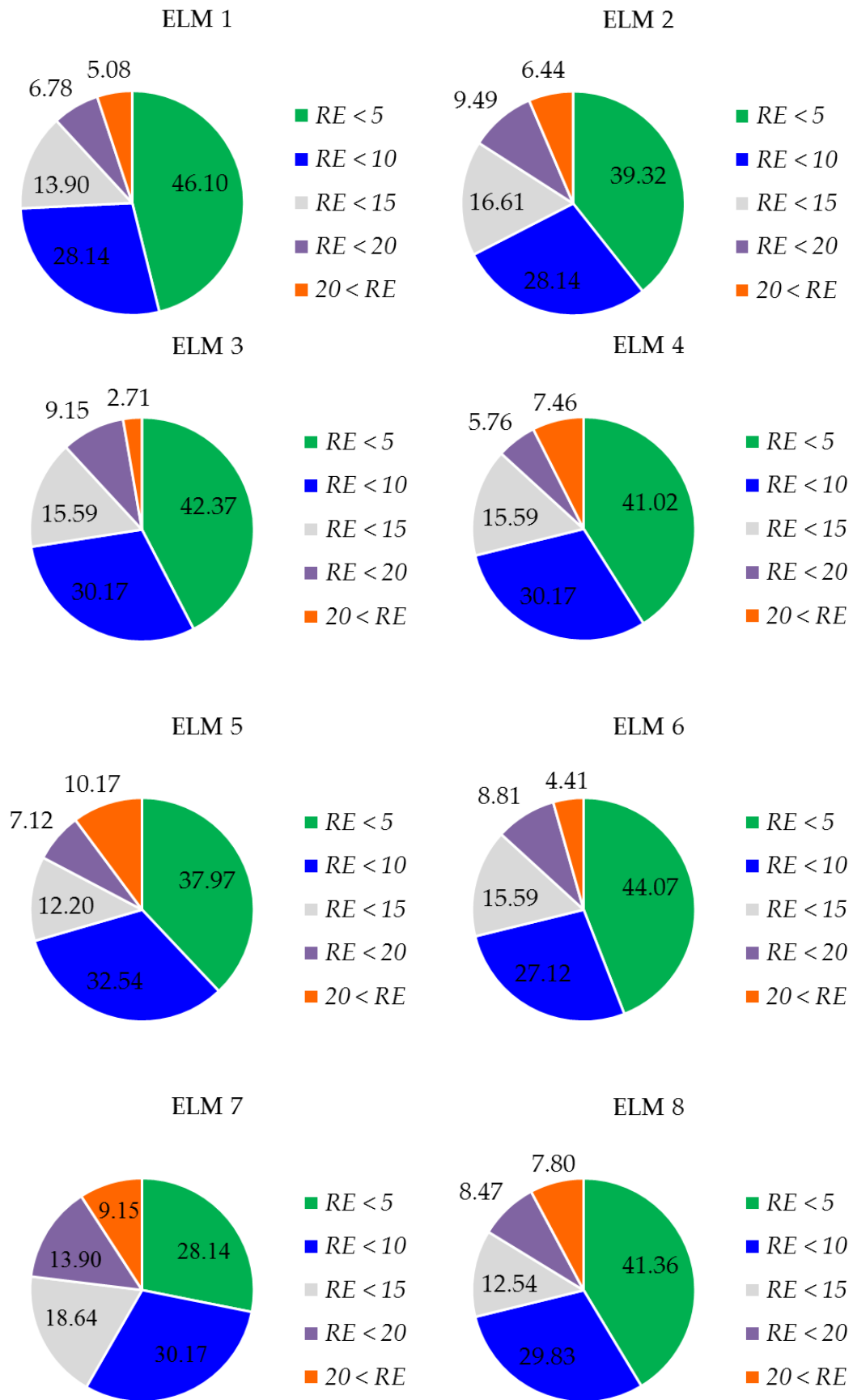


Figure 5. Cont.

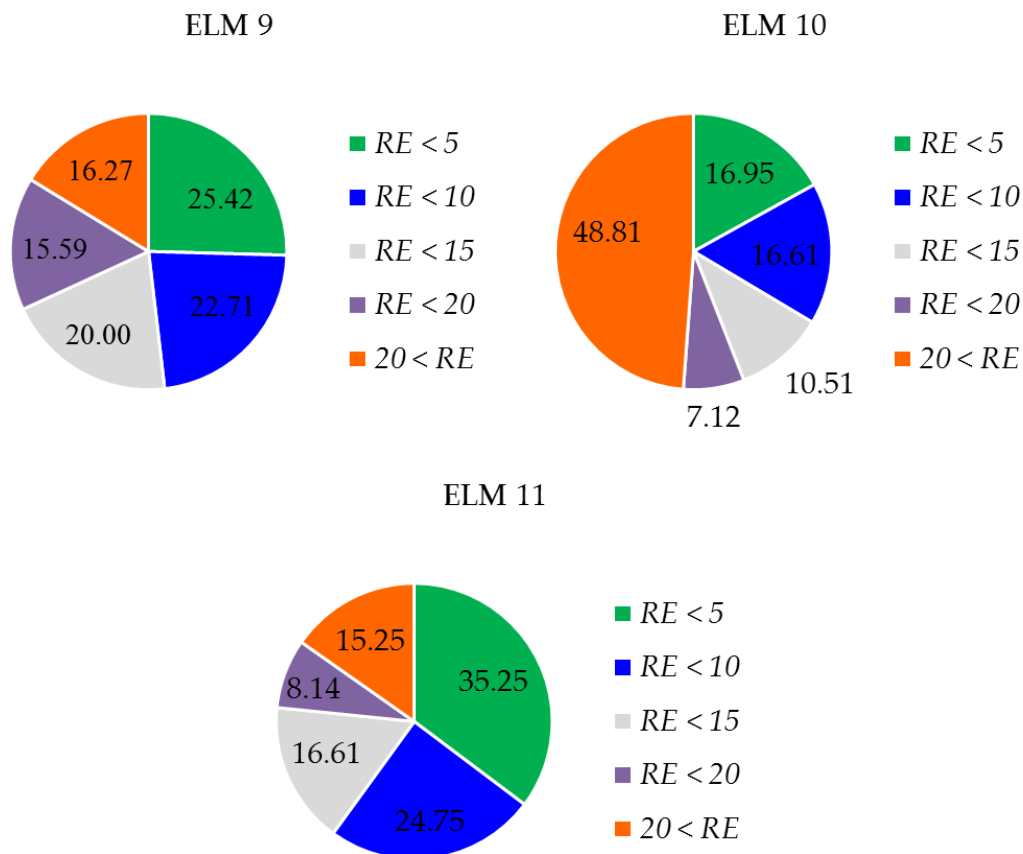


Figure 5. Relative error distribution for different input combinations.

The ELM3 input combination did not include the effect of input variable d_{50}/L on relative scour depth. By eliminating the effect of d_{50}/L on the abutment scour depth, the accuracy of scour depth estimation reduced, and this increased the $RMSE$ compared to ELM1 ($R = 0.96$, $RMSE = 0.177$). ELM4 included parameters d_{50}/L , K_s , and F_e as the input combination. The statistical indices signified that eliminating the relative flow depth parameter led to an over 1% increase in mean relative error ($MAPE = 9.29$) over the model that includes all effective parameters in scour depth estimation ($MAPE = 7.69$).

Thus, it could be concluded that the incoming flow around abutments was an effective parameter in relative scour depth (d_s/L) estimation. By eliminating the parameter F_e from the relative scour depth estimation (ELM5), the mean relative error ($MAPE = 9.14$) and the root mean square error ($RMSE = 0.226$) increased more than ELM1. Among models with three input variables, model five exhibited the weakest performance. In fact, among the four dimensionless parameters in Equation (14), parameter F_e appeared to be the most effective parameter on d_s/L estimation. The results of RE distribution for ELM3 to ELM6 showed that the percentage of the estimated samples with less than 5% and 10% in these models was less than ELM1. It should be noted that the lower performance to estimate d_s/L was related to ELM5. According to the explanation given, the first rank of the most effective parameters in abutment scour depth predicting was related to F_e , and the h/L , K_s , and d_{50}/L were in the second to fourth rank, respectively.

In estimating d_s/L , ELM6 to ELM11 only used two dimensionless parameters (i.e., from a total of four parameters in Equation (14)). Parameter F_e in ELM6, ELM7, and ELM8 was one of the two constant parameters. Concerning all indices presented in Figure 5 for the three models, in addition to F_e , ELM6 also considered h/L , and most estimated values showed little difference from the observed values ($R = 0.96$). The mean relative error for ELM6 was less than 9% ($MAPE = 8.17\%$). Figure 5 indicates that ELM7 ($RMSE = 0.254$) and ELM8 ($RMSE = 0.327$) exhibited weaker performance than

ELM6 ($RMSE = 0.192$); in addition to F_e , ELM7 considered the impact of d_{50}/L , and the majority of data points had a mean relative error of 14% ($MAPE = 13.1$).

Finally, among models that only considered two parameters in estimating the relative scour depth, ELM6 ($d_s/L = f(F_e, h/L)$) was selected as the best. Among other two-parameter models that did not include parameter F_e , ELM10 performed the worst. This model included the effect of h/L and K_s . ELM10 exhibited the highest scattering and lowest accuracy ($SI = 0.287$, $R = 0.61$), with the majority of data points having a relative error of 24% (Figure 5). The RE distribution indicated that the lowest performance of models with only three input parameters was related to the ELM5 so that only 16.94% of all samples were estimated by this model and had relative error less than 5%.

Based on the given explanation, it could be concluded that in the ELM method, the F_e and h/L parameters were effective inputs on relative scour depth in clear water conditions (when the bed sediment particles are not in motion from upstream toward downstream). On the other hand, not considering the excess abutment Froude number and relative sediment size in relative scour depth estimation led to a significant decrease in accuracy and a significant increase in relative error. According to the results, ELM1 with h/L , d_{50}/L , K_s , and F_e as effective parameters in the estimation of scour depth at abutments was deemed the best ELM model.

To evaluate the proposed ELM model's accuracy in predicting the scour depth around abutments in clear water condition, the performance of the developed ELM-based model was compared with conventional regression-based models [22,23] and recently artificial intelligence (AI) based techniques [46,47] by combined accuracy (CA) index for training and testing phases. The lowest CA at both phases is related to Muzammil [23], who provided his model using conventional nonlinear regression. Another conventional equation is Dey and Barbhuiya [22]. The CA index value of this model ($CA = 0.56$) was almost half the value obtained for the Muzammil [23] model ($CA = 1.27$).

However, there was a significant difference between the performance of regression methods and artificial intelligence methods. In addition to the developed ELM model, Moradi et al. [46] and Azimi et al. [47] models were also classified as AI-based models. Both of these methods were presented based on ANFIS so that the Moradi et al. [46] was provided as classical ANFIS, while the model of Azimi et al. [47] was introduced as a multi-objective evolutionary optimization of ANFIS.

The optimized model [47] performed better than the classical model [46], as shown in Figure 6. The model of Azimi et al. [47] provided excellent results in the training phase, but comparing the accuracy of this model with the ELM in the test phase, which indicated the generalizability of a model, demonstrated the superior performance of the developed ELM. Also, the developed method in the current study not only had a higher accuracy than existing ones but also eliminated the underlying problem of existing AI-based models [46,47] in providing a specific relationship for practical applications.

Figure 7 indicates the Taylor diagram [68] for developed ELM model and conventional regression-based and AI-based techniques by considering the results of the standard deviation. The correlation coefficient and $RMSE$ were provided simultaneously for a model in a single diagram using the Taylor diagram. The very low performance of the conventional regression-based techniques in comparison with the AI-based models and developed ELM was clear. Owing to this figure, the developed ELM model outperformed than existing models (conventional and AI-based models).

Table 3 presents the quantitative evaluation of the uncertainties in the abutment scours depth estimation using the developed ELM model versus the existing ones. It should be noted that the uncertainty analysis (UA) was done for the testing phase [69,70]. To calculate the UA, the individual estimation error (IEE) was $e_j = E_j - T_j$, where E and T are the estimated and target values, respectively. Using IEE, the mean of IEE (MIEE) and standard deviation of IEE (SDIEE) were computed as $\bar{e} = \sum_{j=1}^n e_j$ and $S_e = \sqrt{\sum_{j=1}^n (e_j - \bar{e})^2 / n - 1}$, respectively (where n denotes to a number of the testing samples). The positive (or negative) value of the MIEE indicated that the desired model over-estimated (under-estimated) the target values of the abutment scour depth. In the following, the MIEE and SDIEE

were employed to define confidence bound (CB) by the Wilson score method [71] without continuity correction so that the $\pm 1.96 S_e$ yielded an almost 95% CB.

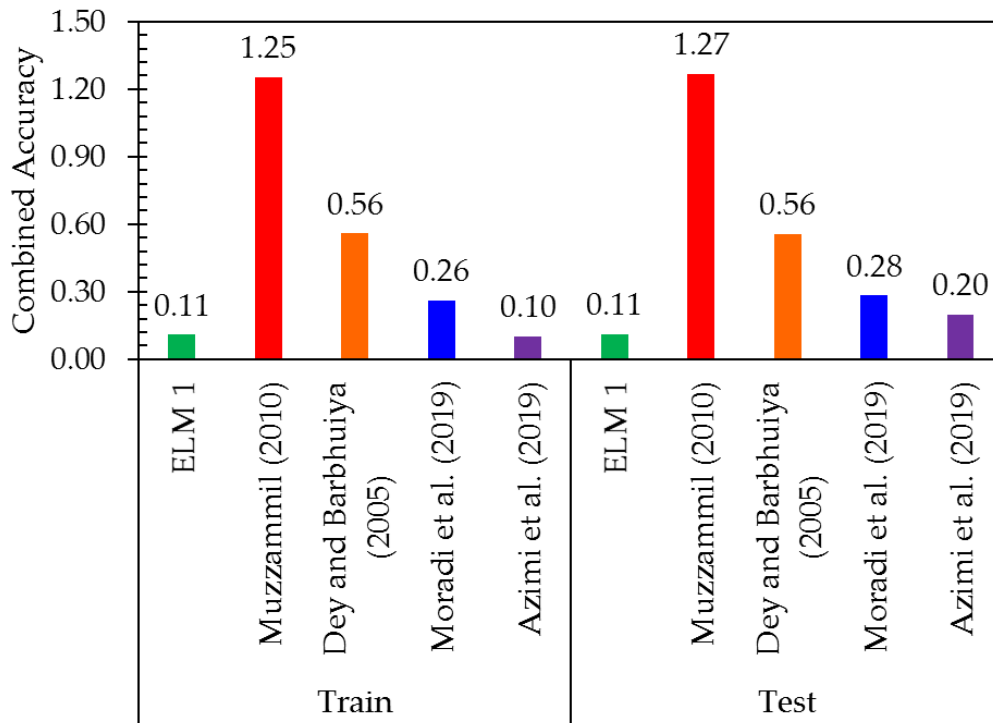


Figure 6. Comparison of the developed ELM model for abutment scour depth prediction with existing conventional and artificial intelligence (AI)-based techniques by combined accuracy (CA) index.

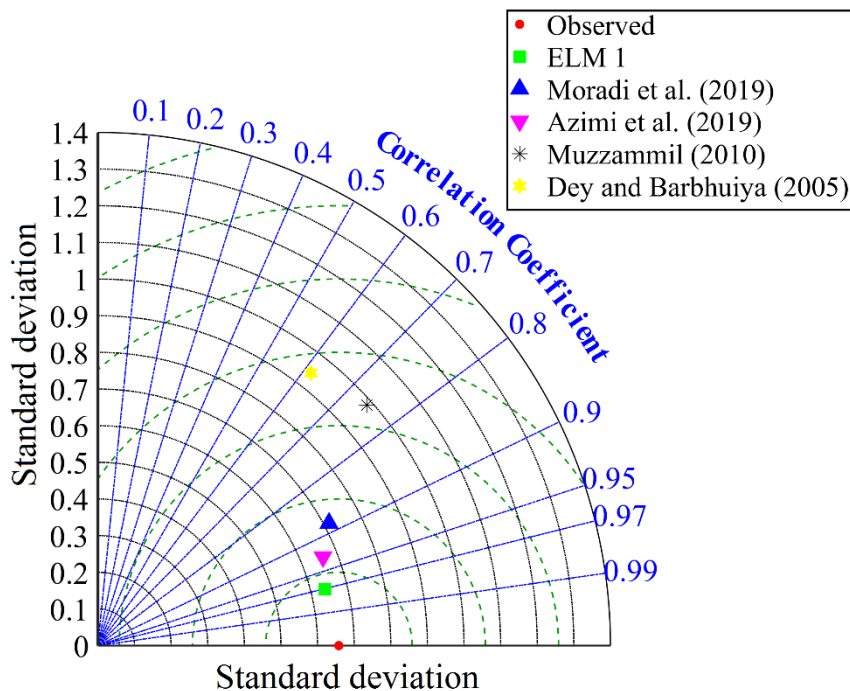


Figure 7. Taylor diagram for developed ELM model and conventional regression-based and AI-based techniques.

Owing to the results of Table 3, it was clear that the developed ELM outperformed than conventional [22,23] and AI-based models [46,47] with the lowest computed uncertainty. The MIEE for

the developed ELM model was computed as +0.001 compared to 0.044, −0.044, −1.613, and −0.171 for Moradi et al. [46], Azimi et al. [47], Muzzammil [23], and Dey and Barbhuiya [22], respectively. It was observed that the developed ELM model and the results of Moradi et al. (2019) over-estimated the abutment scour depth, while the other prediction models underestimated it. Similar to MEE, the lowest value of the standard deviation of estimated error (SDEE), 95% estimation error interval (EEI), and width of uncertainty band (WUB) were related to the developed ELM model.

Table 3. Uncertainty analysis of the developed ELM model versus existing regression and artificial intelligence (AI)-based techniques.

Model	MIEE	SDEE	95% CB	WUB
ELM1	0.001	0.162	(−0.025 0.028)	±0.026
Moradi et al. [46]	0.044	0.344	(−0.012 0.100)	±0.056
Azimi et al. [47]	−0.044	0.304	(−0.093 0.006)	±0.050
Muzzammil [23]	−1.613	0.702	(−1.728 −1.499)	±0.114
Dey and Barbhuiya [22]	−0.171	0.757	(−0.294 −0.047)	±0.123

Note: MIEE, mean of individual estimation error; SDEE, standard deviation of individual estimation error; CB, confidence bound; WUB, width of uncertainty bound.

Due to the best performance of the ELM1 in comparison with other ELM models (ELM2 to ELM11) and existing model, the equation extracted from ELM1, which was selected as the best model in this study, is presented as follows:

$$\frac{d_s}{L} = \left| \left[\frac{1}{(1 + \exp(InW \times InV + BHN))} \right]^T \times OutW \right| \tag{20}$$

where *InW* is the input weight, *InV* is the input variable vector, *BHN* is the bias of hidden neurons, and *OutW* is the output weight. The matrices of each variable in Equation (20) are defined as follows:

$$InV = \begin{bmatrix} Fe \\ \frac{h}{L} \\ \frac{d_{50}}{L} \\ k_s \end{bmatrix} InW = \begin{bmatrix} +0.79 & -0.98 & +0.46 & -0.03 \\ +0.55 & -0.40 & -0.24 & -0.20 \\ +0.65 & -0.75 & -0.35 & -0.77 \\ -0.15 & +0.25 & -0.96 & -0.89 \\ +0.33 & +0.21 & +0.20 & -0.29 \\ +0.62 & +0.37 & -0.33 & +0.26 \\ +0.62 & -0.88 & -0.51 & +0.09 \\ -0.98 & +0.85 & +0.72 & -0.85 \\ -0.80 & +0.29 & +0.46 & +0.89 \\ +0.73 & +0.59 & -0.24 & -0.98 \\ -0.90 & +0.11 & -0.07 & +0.27 \\ -0.98 & -0.24 & -0.75 & +0.87 \\ -0.64 & +0.70 & +0.22 & +0.02 \\ -0.86 & +0.94 & +0.23 & +0.54 \\ +0.42 & -0.84 & +0.07 & +0.10 \\ -0.63 & +0.34 & +0.89 & -0.53 \\ +0.61 & -0.14 & -0.01 & -0.27 \\ +0.02 & +0.24 & +0.48 & -0.20 \\ +0.49 & +0.17 & +0.49 & +0.54 \\ +0.10 & -0.71 & +1.00 & -0.58 \end{bmatrix} OutW = \begin{bmatrix} 7.36 \\ 47.73 \\ 77.48 \\ -267.24 \\ 1998.12 \\ 921.93 \\ -185.62 \\ -138.59 \\ -36.49 \\ -206.82 \\ 57.95 \\ 305.21 \\ 384.68 \\ 46.36 \\ -102.69 \\ 727.28 \\ 192.17 \\ -3163.74 \\ -323.08 \\ 445.98 \end{bmatrix} BHN = \begin{bmatrix} 0.26 \\ 0.91 \\ 0.67 \\ 0.77 \\ 0.14 \\ 0.52 \\ 0.23 \\ 0.37 \\ 0.94 \\ 0.60 \\ 0.16 \\ 0.45 \\ 0.32 \\ 0.35 \\ 0.77 \\ 0.69 \\ 0.22 \\ 0.97 \\ 0.20 \\ 0.44 \end{bmatrix}$$

To evaluate the performance of the developed ELM-based model (Equation (20)) in scour depth prediction, the Ballio et al. [72] dataset was applied. The scatter plot of the predicted relative scours

depth (d_s/l) versus observed ones that were collected from Ballio et al. [72] are provided in Figure 8. Owing to this figure, all samples were estimated with a relative error of less than 10%, so that the means relative error for these samples was less than 5% ($MAPE = 4.407\%$). The other statistical indices related to estimated samples ($R = 0.948$; $RMSE = 0.036$; $SI = 0.05$; $CA = 0.16$) indicated the high prediction level of the developed model at a dataset, which was different from the data employed in model training.

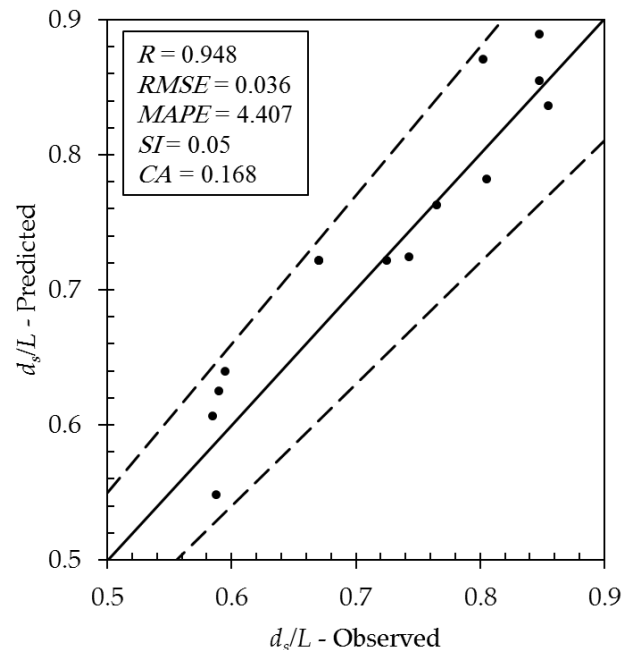


Figure 8. Scatter plot of developed ELM-based model for Ballio et al. [72] model.

4. Discussion

The performance of the ELM machine learning model developed in the current study was compared with conventional models [22,23] and recently developed AI-based techniques [46,47]. The model's performance was examined in terms of five statistical indices of correlation coefficient (R), root means square error ($RMSE$), scatter index (SI), mean absolute percentage error ($MAPE$), and recently introduced combined accuracy (CA). Besides, the comparison of the developed model was also compared with the existing one in terms of the Taylor diagram and uncertainty analysis. The results of all comparisons demonstrated that the developed model provided better performance than conventional and AI-based regression models. Over-fitting is a well-known problem in machine learning modeling. Over-fitting occurred when the developed model fitted exactly through the training stage, leading to low performance of the developed model at unseen samples (i.e., training stage). It is well-known that an organized model with lower adjustable parameters through the training stage could prevent over-fitting challenge. It should be noted that in the current study, data splitting was considered as 50%–50% so that 50% of all samples were randomly selected for training and testing, while the rest of the ones applied to check the performance of the model for unseen samples. The results indicated the high level of accuracy of the developed model at both the training and testing stage simultaneously. Consequently, the developed model in the current study did not experience the over-fitting problem and produced an acceptable prediction for unseen samples in the testing stages. Moreover, the generalizability of the developed model was examined by Ballio et al. [72] dataset, which differed from Dey and Barbhuiya [22] that was applied for training and testing stages.

To investigate the alteration trend of the scour depth around abutment to each input variable provided in the Equation (20) (F_e , h/L , d_{50}/L , k_s), the partial derivative sensitivity analysis (PDSA) was performed [73,74]. In the PDSA, the partial differential of the development model was calculated between output and each input variable, and the results of the partial difference were reported as the

sensitivity of the developed model to x_i input (in the current study, $i = 1, 2, 3, 4$). The positive (or negative) value of the sensitivity demonstrated that an increase in the x_i resulted in an increase (or decrease) in the output variable. Besides, the high (or low) value of the sensitivity implied the higher (or lower) efficiency of the x_i on the output variable.

Figure 9 indicates the results of the PDSA of developed ELM-based model (Equation (20)) to input variables ($F_e, h/L, d_{50}/L, K_s$). All of the sensitivity values for F_e were positive. Indeed, the increasing (or decreasing) of the F_e led to enhance (or reduction) the d_s/L . The highest value of sensitivity of the model to F_e was related to the lower value of these variables. The sensitivity value for F_e indicated that the developed ELM model was the most sensitive to F_e in comparison to others. Similar to F_e , the highest sensitivity for h/L and d_{50}/L attained at the lowest value of each variable. The sensitivity sign in the h/L was not constant, so the trend of the developed ELM model to h/L alteration was not clear, while, for most samples, an increasing (or decreasing) in the d_{50}/L resulted to reduction (or enhancing) of the output variable. The results of PDSA for K_s were similar to h/L without any constant alteration trend.

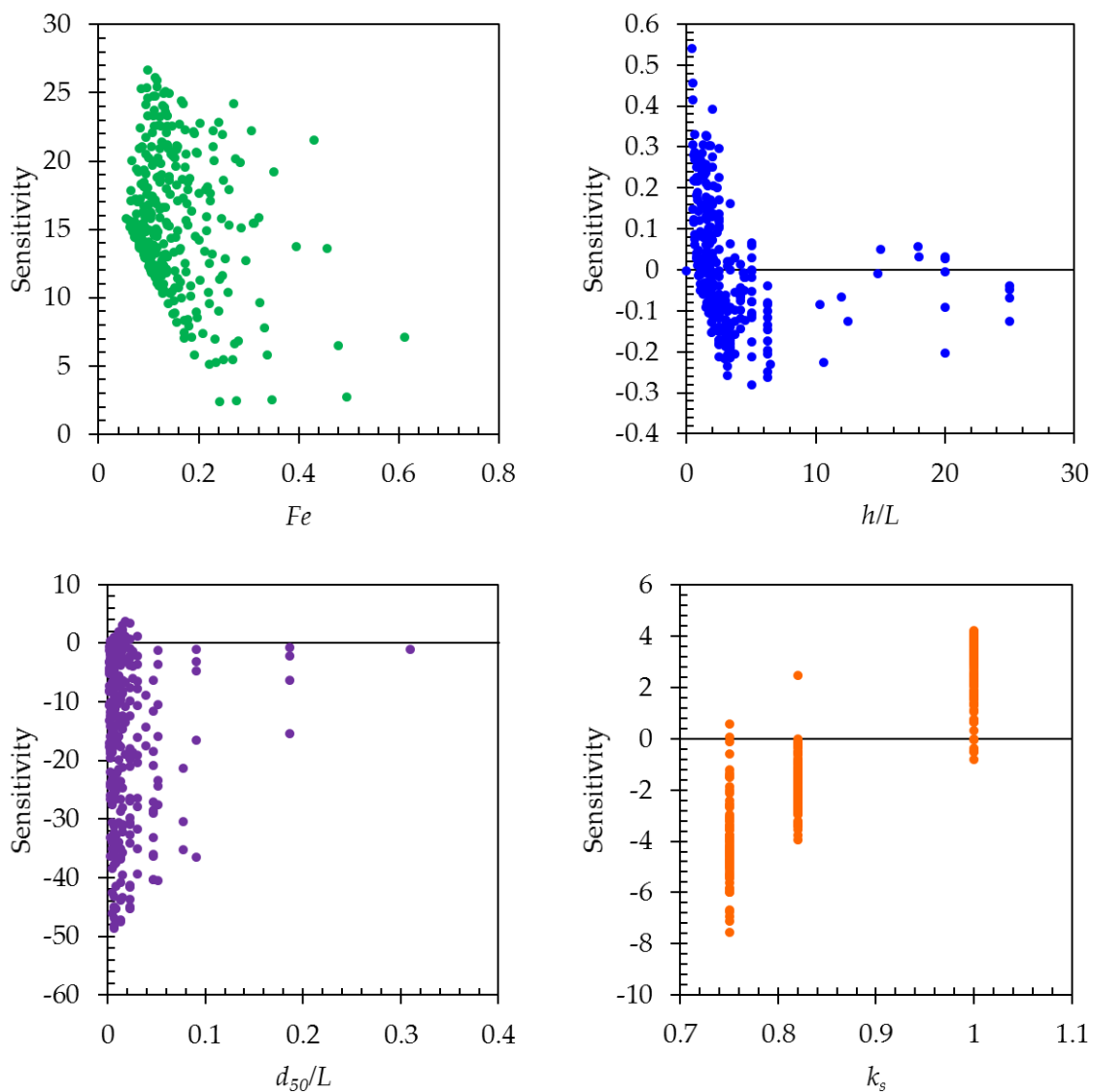


Figure 9. Partial derivative sensitivity analysis (PDSA) results for each input variable in the developed ELM-based model.

Figure 10 represents the effect of altering the input variables on the compressibility indices. This was accomplished by changing one of the input variable (i.e., $F_e, h/L, d_{50}/L, k_s$) at a constant rate (−10 to

10%), while the other ones were constant. The *MAPE* of the developed ELM model in abutment scours depth estimation was calculated for each input variable variations in the defined range. Figure 10 shows that the compressibility indices estimated by the developed ELM model were significantly affected by an error in measuring F_e and k_s so that the *MAPE* increased drastically. For instance, a 10% error in measuring F_e and K_s resulted in more than 14% *MAPE*, which was more than two times the *MAPE* for applying these variables without measuring error. In contrast, the error in measuring h/L and d_{50}/L was not significant, so the 10% error in measuring h/L and d_{50}/L led to increasing the *MAPE* less than 1% related to applying these variables without any measuring error.

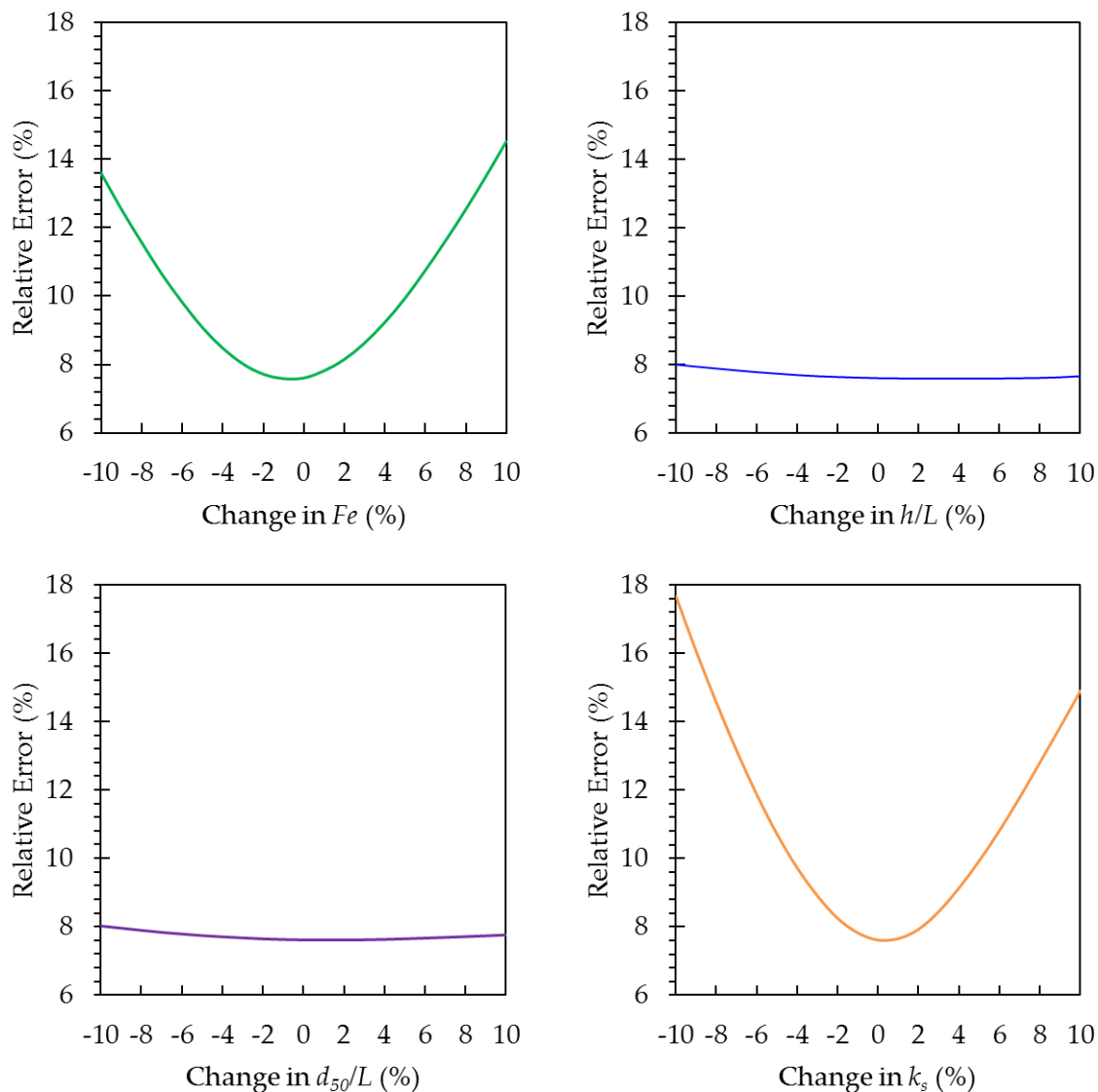


Figure 10. Alteration effect of the input variables on the output mean absolute percentage error (*MAPE*).

5. Conclusions

According to the significance of scour at bridge abutments and the prevention of damage caused by incorrect scour depth estimation, the local scour depth at abutments in clear water was studied in this work using extreme learning machines (ELM). The results of this study are presented below.

- Predicting the normalized scour depth over abutment length (d_s/L) at bridge abutments in clear water condition and on a uniform sediment bed was a function of relative depth (h/L), excess abutment Froude number (F_e), relative sediment size (d_{50}/L), and the structure's geometric coefficient (K_s).

- Among the nonlinear activation functions used in extreme learning machines, the sigmoid activation function exhibited good accuracy ($R = 0.97$) and mean error below 8% ($MAPE = 7.69\%$) in estimating the scour depth at bridge abutments.
- Among the four parameters affecting scour depth, elimination of F_e and d_{50}/L led to a 24% increase in relative error ($MAPE = 23.57$). The combination of h/L and F_e performed the best compared to the other two-parameter models.
- According to the ELM method, Model 1 that included all parameters (F_e , d_{50}/L , K_s , h/L) for predicting the relative scour depth around abutments embedded on a bed with uniform materials in clear water condition was deemed the best model.
- The best ELM model (ELM1) predicted the relative scour depth around abutments with greater accuracy than the conventional regression and AI-based techniques.

Supplementary Materials: The following are available online at <http://www.mdpi.com/2073-4441/12/1/301/s1>. Table S1: $MAPE$, $RMSE$, R and SI values of different input combinations in abutment scour depth prediction, Table S2: Relative error (RE) values for different input combinations verified in this study.

Author Contributions: Conceptualization, H.B. and F.M.; methodology, H.B., F.M. and I.E.; formal analysis, F.M. and I.E.; visualization, F.M., A.A.S. and A.H.A.; writing—original draft preparation, H.B., F.M. and I.E.; writing—review and editing, H.B., A.A.S., A.H.A., B.G. and A.R.-P.; project administration, H.B. All authors have read and agreed to the published version of the manuscript.

Funding: This research was funded by The Natural Sciences and Engineering Research Council of Canada.

Conflicts of Interest: The authors declare no conflict of interest.

References

1. Melville, B.W.; Sutherland, A.J. Design method for local scour at bridge piers. *J. Hydraul. Eng.* **1988**, *114*, 1210–1226. [[CrossRef](#)]
2. Macky, G.H. *Survey of Roading Expenditure Due to Scour*; C.R. 90.09; Department of Scientific and Industrial Research (DSIR) Hydrology Centre: Christchurch, New Zealand, 1990.
3. Cardoso, A.H.; Bettess, R. Effects of time and channel geometry on scour at bridge abutments. *J. Hydraul. Eng.* **1999**, *125*, 388–399. [[CrossRef](#)]
4. Azamathulla, H.M.; Ghani, A.A.; Zakaria, N.A.; Guven, A. Genetic programming to predict bridge pier scour. *J. Hydraul. Eng.* **2009**, *136*, 165–169. [[CrossRef](#)]
5. Ghazvinei, P.T.; Mohamed, T.A.; Ghazali, A.H.; Huat, B.K. Scour hazard assessment and bridge abutment instability analysis. *Electron. J. Geotech. Eng.* **2012**, *17*, 2213–2224.
6. Lim, S.Y. Equilibrium clear-water scour around an abutment. *J. Hydraul. Eng.* **1997**, *123*, 237–243. [[CrossRef](#)]
7. Kwan, T.F. *A Study of Abutment Scour*; University of Auckland: Auckland, New Zealand, 1988.
8. May, R.W.; Ackers, J.C.; Kirby, A.M. *Manual on Scour at Bridges and Other Hydraulic Structures*; Pub. No. 551; Construction Industry Research and Information Association: London, UK, 2002.
9. Hosseini, K.; Karami, H.; Hosseinjanzadeh, H.; Ardeshir, A. Prediction of time-varying maximum scour depth around short abutments using soft computing methodologies-A comparative study. *KSCE J. Civ. Eng.* **2015**, *20*, 2070–2081. [[CrossRef](#)]
10. Manzouri, M.; Azimi, A.H. Laboratory experiments evaluating sedimentation and mound formation of obliquely discharged sand particles in stagnant water. *Int. J. Sediment Res.* **2019**, *34*, 564–576. [[CrossRef](#)]
11. Azimi, A.H.; Qian, Y.; Zhu, D.Z.; Rajaratnam, N. An experimental study on circular slurry wall jets. *Int. J. Multiph. Flow* **2015**, *74*, 34–44. [[CrossRef](#)]
12. Laursen, E.M. Analysis of relief bridge scour. *J. Hydraul. Div.* **1963**, *89*, 93–118.
13. Gill, M.A. Erosion of sand beds around spur dikes. *J. Hydraul. Div. ASCE* **1972**, *98*, 1587–1602.
14. Tey, C.B. *Local Scour at Bridge Abutments*; University of Auckland: Auckland, New Zealand, 1984.
15. Azimi, A.H.; Zhu, D.Z.; Rajaratnam, N. An experimental study of sand deposition from slurry wall jets. *J. Eng. Mech. ASCE* **2014**, *140*, 296–314. [[CrossRef](#)]
16. Melville, B.W. Local scour at bridge abutments. *J. Hydraul. Eng.* **1992**, *118*, 615–631. [[CrossRef](#)]
17. Dey, S.; Barbhuiya, A.K. Clear water scour at abutments. *Proc. Inst Civ Eng. Water Manag.* **2004**, *157*, 77–97. [[CrossRef](#)]

18. Fael, C.M.; Simarro-Grande, G.; Martín-Vide, J.P.; Cardoso, A.H. Local scour at vertical-wall abutments under clear-water flow conditions. *Water Resour. Res.* **2006**, *42*, W10408. [[CrossRef](#)]
19. Abou-Seida, M.M.; Elsaeed, G.H.; Mostafa, T.M.; Elzahry, E.F. Local scour at bridge abutments in cohesive soil. *J. Hydraul. Res.* **2012**, *50*, 171–180. [[CrossRef](#)]
20. Kumcu, S.Y.; Kokpinar, M.A.; Gogus, M. Scour protection around vertical-wall bridge abutments with collars. *KSCE J. Civ. Eng.* **2014**, *18*, 1884–1895. [[CrossRef](#)]
21. Barbhuiya, A.K.; Mazumder, M.H. Live-bed local scour around vertical-wall abutments. *ISH J. Hydraul. Eng.* **2014**, *20*, 339–351. [[CrossRef](#)]
22. Dey, S.; Barbhuiya, A.K. Time variation of scour at abutments. *J. Hydraul. Eng.* **2005**, *131*, 11–23. [[CrossRef](#)]
23. Muzzammil, M. ANFIS approach to the scour depth prediction at a bridge Abutment. *J. Hydroinformatics* **2010**, *12*, 474–485. [[CrossRef](#)]
24. Ettema, R.; Melville, B.W.; Barkdoll, B. Scale effect in pier-scour experiments. *J. Hydraul. Eng.* **1998**, *124*, 639–642. [[CrossRef](#)]
25. Bateni, S.M.; Borghei, S.M.; Jeng, D.S. Neural network and neuro-fuzzy assessments for scour depth around bridge piers. *Eng. Appl. Artif. Intell.* **2007**, *20*, 401–414. [[CrossRef](#)]
26. Zanganeh, M.; Yeganeh-Bakhtiary, A.; Yamashita, T. ANFIS and ANN models for the estimation of wind and wave-induced current velocities at Joesutsu-Ogata coast. *J. Hydroinformatic.* **2016**, *18*, 371–391. [[CrossRef](#)]
27. Khan, M.; Azamathulla, H.M.; Tufail, M. Gene-expression programming to predict pier scour depth using laboratory data. *J. Hydroinformatic.* **2012**, *14*, 628–645. [[CrossRef](#)]
28. Azamathulla, H.M. Gene-expression programming to predict scour at a bridge abutment. *J. Hydroinformatic.* **2012**, *14*, 324–331. [[CrossRef](#)]
29. Roushangar, K.; Akhgar, S.; Erfan, A.; Shiri, J. Modeling scour depth downstream of grade-control structures using data driven and empirical approaches. *J. Hydroinformatic.* **2016**, *18*, 946–960. [[CrossRef](#)]
30. Azimi, H.; Bonakdari, H.; Ebtehaj, I.; Ashraf Talesh, S.H.; Jamali, A. Evolutionary Pareto Optimization of an ANFIS Network for Modeling Scour at Pile Groups in Clear Water Condition. *Fuzzy Sets Syst.* **2016**, *319*, 50–69. [[CrossRef](#)]
31. Sharafi, H.; Ebtehaj, I.; Bonakdari, H.; Zaji, A.H. Design of a Support Vector Machine with Different Kernel Functions to Predict Scour Depth around Bridge Piers. *Nat. Hazards* **2016**, *84*, 2145–2162. [[CrossRef](#)]
32. Najafzadeh, M.; Barani, G.A.; Azamathulla, H.M. Prediction of pipeline scour depth in clear-water and live-bed conditions using group method of data handling. *Neural Comput. Appl.* **2014**, *24*, 629–635. [[CrossRef](#)]
33. Najafzadeh, M.; Barani, G.A.; Hessami-Kermani, M.R. Group method of data handling to predict scour at downstream of a ski-jump bucket spillway. *Earth Sci. Inf.* **2014**, *7*, 231–248. [[CrossRef](#)]
34. Najafzadeh, M.; Barani, G.A.; Kermani, M.R. GMDH based back propagation algorithm to predict abutment scour in cohesive soils. *Ocean Eng.* **2013**, *59*, 100–106. [[CrossRef](#)]
35. Najafzadeh, M.; Lim, S.Y. Application of improved neuro-fuzzy GMDH to predict scour depth at sluice gates. *Earth Sci. Inf.* **2015**, *8*, 187–196. [[CrossRef](#)]
36. Etemad-Shahidi, A.; Bonakdar, L.; Jeng, D.S. Estimation of scour depth around circular piers: Applications of model tree. *J. Hydroinformatic.* **2015**, *17*, 226–238. [[CrossRef](#)]
37. Bateni, S.M.; Jeng, D.S. Estimation of pile group scour using adaptive neuro-fuzzy approach. *Ocean Eng.* **2007**, *34*, 1344–1354. [[CrossRef](#)]
38. Muzzammil, M. Application of neural networks to scour depth prediction at the bridge abutments. *Eng. Appl. Comput. Fluid Mech.* **2008**, *2*, 30–40. [[CrossRef](#)]
39. Ghani, A.A.; Azamathulla, H. Gene-expression programming for sediment transport in sewer pipe systems. *J. Pipeline Syst. Eng. Pract.* **2010**, *2*, 102–106.
40. Begum, S.A.; Fujail, A.M.; Barbhuiya, A.K. Artificial neural network to predict equilibrium local scour depth around semicircular bridge abutments. In Proceedings of the 6th SASTech, Kuala Lumpur, Malaysia, 24–25 March 2012; Organized by Khavaran Institute of Higher Education: Kuala Lumpur, Malaysia, 2012.
41. Zamani, A.; Sorbi, M.R.; Safavi, A.A. Application of neural network and ANFIS model for earthquake occurrence in Iran. *Earth Sci. Inf.* **2013**, *6*, 71–85. [[CrossRef](#)]
42. Mehr, A.D.; Kahya, E.; Bagheri, F.; Deliktas, E. Successive-station monthly streamflow prediction using neuro-wavelet technique. *Earth Sci. Inf.* **2014**, *7*, 217–229. [[CrossRef](#)]

43. Hassan, M.; Shamim, M.A.; Hashmi, H.N.; Ashiq, S.Z.; Ahmed, I.; Pasha, G.A.; Naeem, U.A.; Ghumman, A.R.; Han, D. Predicting streamflows to a multipurpose reservoir using artificial neural networks and regression techniques. *Earth Sci. Inf.* **2015**, *8*, 337–352. [[CrossRef](#)]
44. Ebtehaj, I.; Bonakdari, H.; Gharabaghi, B. Closure to “An integrated framework of Extreme Learning Machines for predicting scour at pile groups in clear water condition by Ebtehaj, I., Bonakdari, H., Moradi, F., Gharabaghi, B., Khozani, Z.S.”. *Coast. Eng.* **2019**, *147*, 135–137. [[CrossRef](#)]
45. Ebtehaj, I.; Bonakdari, H.; Shamshirband, S.; Ismail, Z.; Hashim, R. New Approach to Estimate Velocity at Limit of Deposition in Storm Sewers Using Vector Machine Coupled with Firefly Algorithm. *J. Pipeline Syst. Eng. Pract.* **2016**, *20*, 04016018. [[CrossRef](#)]
46. Moradi, F.; Bonakdari, H.; Kisi, O.; Ebtehaj, I.; Shiri, J.; Gharabaghi, B. Abutment scour depth modeling using neuro-fuzzy-embedded techniques. *Mar. Georesour. Geotechnol.* **2019**, *37*, 190–200. [[CrossRef](#)]
47. Azimi, H.; Bonakdari, H.; Ebtehaj, I.; Shabanlou, S.; Talesh, S.H.A.; Jamali, A. A pareto design of evolutionary hybrid optimization of ANFIS model in prediction abutment scour depth. *Sādhanā* **2019**, *44*, 169–182. [[CrossRef](#)]
48. Huang, G.B.; Zhou, H.; Ding, X.; Zhang, R. Extreme learning machine for regression and multiclass classification. *IEEE Trans. Syst. Man Cyber Part B* **2012**, *42*, 513–529. [[CrossRef](#)] [[PubMed](#)]
49. Huang, G.B.; Zhu, Q.Y.; Siew, C.K. Extreme learning machine: Theory and applications. *Neurocomputing* **2006**, *70*, 489–501. [[CrossRef](#)]
50. Cheng, G.J.; Cai, L.; Pan, H.X. Comparison of Extreme Learning Machine with Support Vector Regression for Reservoir Permeability Prediction. *Comput. Intell. Secur.* **2009**, *2*, 173–176.
51. Ebtehaj, I.; Bonakdari, H.; Shamshirband, S. Extreme learning machine assessment for estimating sediment transport in open channels. *Eng. Comput.* **2016**, *32*, 691–704. [[CrossRef](#)]
52. Naganna, S.R.; Deka, P.C.; Ghorbani, M.A.; Biazar, S.M.; Al-Ansari, N.; Yaseen, Z.M. Dew point temperature estimation: Application of artificial intelligence model integrated with nature-inspired optimization algorithms. *Water* **2019**, *11*, 742. [[CrossRef](#)]
53. Niu, W.J.; Feng, Z.K.; Feng, B.F.; Min, Y.W.; Cheng, C.T.; Zhou, J.Z. Comparison of multiple linear regression; artificial neural network; extreme learning machine; and support vector machine in deriving operation rule of hydropower reservoir. *Water* **2019**, *11*, 88. [[CrossRef](#)]
54. Ren, J.; Ren, B.; Zhang, Q.; Zheng, X. A Novel Hybrid Extreme Learning Machine Approach Improved by K Nearest Neighbor Method and Fireworks Algorithm for Flood Forecasting in Medium and Small Watershed of Loess Region. *Water* **2019**, *11*, 1848. [[CrossRef](#)]
55. Zhu, R.; Yang, L.; Liu, T.; Wen, X.; Zhang, L.; Chang, Y. Hydrological Responses to the Future Climate Change in a Data Scarce Region; Northwest China: Application of Machine Learning Models. *Water* **2019**, *11*, 1588. [[CrossRef](#)]
56. Bhasin, V.; Bedi, P.; Singh, N.; Aggarwal, C. FS-EHS: Harmony Search Based Feature Selection Algorithm for Steganalysis Using ELM. In *Innovations in Bio-Inspired Computing and Applications. Advances in Intelligent Systems and Computing*; Snášel, V., Abraham, A., Krömer, P., Pant, M., Muda, A., Eds.; Springer: Cham, Switzerland, 2016; Volume 424.
57. Shen, Y.; Xu, J.; Li, H.; Xiao, L. ELM-based spectral-spatial classification of hyperspectral images using bilateral filtering information on spectral band-subsets. In Proceedings of the IEEE International Geoscience and Remote Sensing Symposium (IGARSS), Beijing, China, 10–15 July 2016; pp. 497–500.
58. Ebtehaj, I.; Bonakdari, H. A Comparative Study of Extreme Learning Machines and Support Vector Machines in Prediction of Sediment Transport in Open Channels. *Int. J. Eng. Ttrans. B Appl.* **2016**, *29*, 1523–1530.
59. Huang, G.B.; Chen, L.; Siew, C.K. Universal approximation using incremental constructive feedforward networks with random hidden nodes. *IEEE Trans. Neural Netw. Learn. Syst.* **2006**, *17*, 879–892. [[CrossRef](#)] [[PubMed](#)]
60. Liang, N.Y.; Huang, G.B.; Saratchandran, P.; Sundararajan, N. A fast and accurate online sequential learning algorithm for feedforward networks. *IEEE Trans. Neural Netw. Learn. Syst.* **2006**, *17*, 1411–1423. [[CrossRef](#)] [[PubMed](#)]
61. Raudkivi, A.J.; Etema, R. Clear-water scour at cylindrical piers. *J. Hydraul. Eng.* **1983**, *109*, 338–350. [[CrossRef](#)]
62. Sheppard, D.M.; Odeh, M.; Glasser, T. Large scale clear-water local pier scour experiments. *J. Hydraul. Eng.* **2004**, *130*, 957–963. [[CrossRef](#)]

63. Firat, M.; Gungor, M. Generalized regression neural networks and feedforward neural networks for prediction of scour depth around bridge piers. *Adv. Eng. Softw.* **2009**, *40*, 731–737. [[CrossRef](#)]
64. Azamathulla, H.; Abghani, A.M.; Zakaria, N.A. An ANFIS based approach for predicting the scour below Flip-Bucket spillway. In Proceedings of the 2nd International Conference on Managing River in the 21st Century: Solution towards Sustainable River Basins, Riverside Kuching, Sarawak, 6–8 June 2007.
65. Yasa, R.; Etemad-Shahidi, A. Classification and regression trees approach for predicting current-induced scour depth under pipelines. *J. Offshore Mech. Arct. Eng.* **2014**, *136*, 011702. [[CrossRef](#)]
66. Najafzadeh, M.; Etemad-Shahidi, A.; Lim, S.Y. Scour prediction in long contractions using ANFIS and SVM. *Ocean Eng.* **2016**, *111*, 128–135. [[CrossRef](#)]
67. Eray, O.; Mert, C.; Kisi, O. Comparison of multi-gene genetic programming and dynamic evolving neural-fuzzy inference system in modeling pan evaporation. *Hydrol. Res.* **2018**, *49*, 1221–1233. [[CrossRef](#)]
68. Taylor, K.E. Summarizing multiple aspects of model performance in a single diagram. *J. Geophys. Res. Atmos.* **2001**, *106*, 7183–7192. [[CrossRef](#)]
69. Ebtehaj, I.; Sattar, A.M.; Bonakdari, H.; Zaji, A.H. Prediction of scour depth around bridge piers using self-adaptive extreme learning machine. *J. Hydroinformat.* **2016**, *19*, 207–224. [[CrossRef](#)]
70. Khozani, Z.S.; Bonakdari, H.; Ebtehaj, I. An analysis of shear stress distribution in circular channels with sediment deposition based on Gene Expression Programming. *Int. J. Sediment Res.* **2017**, *32*, 575–584. [[CrossRef](#)]
71. Newcombe, R.G. Interval estimation for the difference between independent proportions: Comparison of eleven methods. *Stat. Med.* **1998**, *17*, 873–890. [[CrossRef](#)]
72. Ballio, F.; Teruzzi, A.; Radice, A. Constriction effects in clear-water scour at abutments. *J. Hydraul. Eng.* **2009**, *135*, 140–145. [[CrossRef](#)]
73. Azimi, H.; Bonakdari, H.; Ebtehaj, I.; Gharabaghi, B.; Khoshbin, F. Evolutionary design of generalized group method of data handling-type neural network for estimating the hydraulic jump roller length. *Acta Mech.* **2018**, *229*, 1197–1214. [[CrossRef](#)]
74. Gholami, A.; Bonakdari, H.; Zeynoddin, M.; Ebtehaj, I.; Gharabaghi, B.; Khodashenas, S.R. Reliable method of determining stable threshold channel shape using experimental and gene expression programming techniques. *Neural Comput. Appl.* **2019**, *31*, 5799–5817. [[CrossRef](#)]



© 2020 by the authors. Licensee MDPI, Basel, Switzerland. This article is an open access article distributed under the terms and conditions of the Creative Commons Attribution (CC BY) license (<http://creativecommons.org/licenses/by/4.0/>).